

Tangqing Kuang\*, Chuncong Yu, Baiping Xu and Lih-Sheng Turng\*

# Experimental study of penetration interfaces in the overflow fluid-assisted co-injection molding process

DOI 10.1515/polyeng-2014-0369

Received December 17, 2014; accepted May 31, 2015; previously published online August 15, 2015

**Abstract:** The fluid-assisted co-injection molding (FACIM) process can be used to produce hollow plastic products with outer and inner layers. It can be divided into two categories: water-assisted co-injection molding (WACIM) and gas-assisted co-injection molding (GACIM). An experimental study of penetration interfaces in overflow FACIM was carried out based on a lab-developed FACIM system. High-density polyethylene and polypropylene were used as the outer layer and inner layer plastics, respectively, in the experiments and the injection sequence was reversible. Six cross-section cavities were investigated in the experiments. The penetration behaviors of water and gas in different sequences and cavities were compared and analyzed. The penetration interfaces were characterized by the residual wall thickness (RWT). The experimental results showed that the RWT of the inner layer in WACIM fluctuated along the flow direction, while that in GACIM was more even. The difference of viscosity between the outer and inner layer melts affected the stability of the interface between them. The penetration sections of the inner layer and the gas were closer to the cavity sections in GACIM, while the penetration sections of the inner layer and the water were closer to the circular forms in WACIM.

**Keywords:** experimental study; fluid-assisted co-injection molding; overflow; penetration interface; residual wall thickness.

\*Corresponding authors: **Tangqing Kuang**, School of Mechanical and Electrical Engineering, East China Jiaotong University, Nanchang 330013, China, e-mail: kuangtq@aliyun.com; and **Lih-Sheng Turng**, Polymer Engineering Center, University of Wisconsin-Madison, Madison, WI 53706, USA, e-mail: turng@engr.wisc.edu  
**Chuncong Yu**: Product Development Center of Jiangling Motors Co. Ltd., Nanchang 330001, China  
**Baiping Xu**: Technology Development Center for Polymer Processing Engineering, Guangdong Colleges and Universities, Guangdong Industry Technical College, Guangzhou 510641, China

## 1 Introduction

Fluid-assisted co-injection molding (FACIM), an innovative plastic injection molding technology first developed in Germany one decade ago, can be used to produce hollow plastic parts with a multilayer structure [1]. FACIM can be considered a combined processing technology, combining the fluid-assisted injection molding (FAIM) [2–6] and co-injection molding (CIM) processes. According to the fluid it uses, it can be divided into two categories: water-assisted co-injection molding (WACIM) and gas-assisted co-injection molding (GACIM). Based on whether or not the melts completely fill the cavity before fluid injection, FACIM can be categorized into two types: short-shot FACIM (S-FACIM) and overflow FACIM (O-FACIM). In the S-FACIM process, the mold cavity is partially filled with two different polymer melts that are injected sequentially and form a skin/core structure, followed by the injection of fluid into the core of the polymer melt. Figure 1A shows a schematic diagram of the S-FACIM process. S-FACIM parts have some defects such as a switchover mark on the product surface and obvious uneven residual wall thicknesses (RWT) in the flow direction. In the O-FACIM process, the mold cavity is first completely filled with the polymer melt, followed by the injection of high-pressure fluid that pushes the material into an overflow cavity. Figure 1B shows a schematic diagram the O-FACIM process.

FAIM can enable greater freedom of design, material savings, weight reduction, and cost savings in tooling and press capacity requirements [4]. CIM can be used to produce parts with special characteristics by the combination of two or more types of plastic materials, such as using the outer material to achieve required surface properties, while using the core material to obtain sufficient mechanical properties or to reduce cost [7, 8]. FACIM has the advantages of both FAIM and CIM. Moreover, it offers a wide processing window [1]. Currently, FACIM technology is mainly used for automotive, household, and furniture items, highlighting a bright future for FACIM with regard to market prospects.

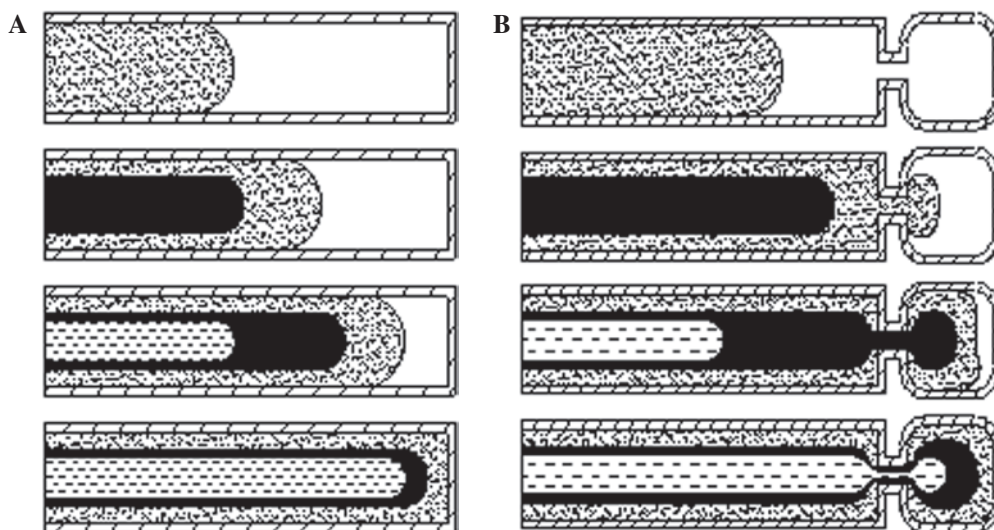


Figure 1: Schematic diagram of FACIM processes: (A) S-FACIM and (B) O-FACIM.

Despite all of the advantages associated with FACIM, the process control of FACIM is more critical and difficult due to its complexity. It is well known that the penetration interface, which affects the RWT, is vital for determining product quality. While some literature is available regarding the penetration interface in FAIM [2, 3, 5–7] and CIM [8, 9], and some investigations of the influence of processing parameters – such as melt temperature, fluid injection delay time, fluid pressure, fluid temperature, and mold temperature – on FACIM via numerical simulation have been reported [10–18], experimental research on the penetration interfaces of FACIM has been rare. Zhou et al. [19] investigated penetration interfaces in a GACIM thick plate. To the best of the authors' knowledge, no one has ever studied penetration interfaces in an FACIM rib.

The present report is devoted to studying penetration interfaces in an O-FACIM rib based on a lab-developed FACIM experimental platform. The influence of the fluid, the polymer rheology, and the shape of the cross-section of the cavity on penetration interfaces in an O-FACIM rib was investigated.

## 2 Materials and methods

### 2.1 Materials

In the experiments, high-density polyethylene (HDPE, Grade DMDA-8008, Dushanzi Petrochemical Co., China) and polypropylene (PP, Grade 1102K, Jinxi Petrochemical Co., China) were used as outer and inner materials,

respectively. In order to identify the interface between the HDPE and PP melt, black and red colorants were added, respectively. Tables 1 and 2 list the characteristics of the HDPE and PP, respectively. The injection sequence of the melts can be reversed to investigate the influence of polymer rheology on the penetration interfaces of the inner melt and the fluid.

### 2.2 Equipment setup

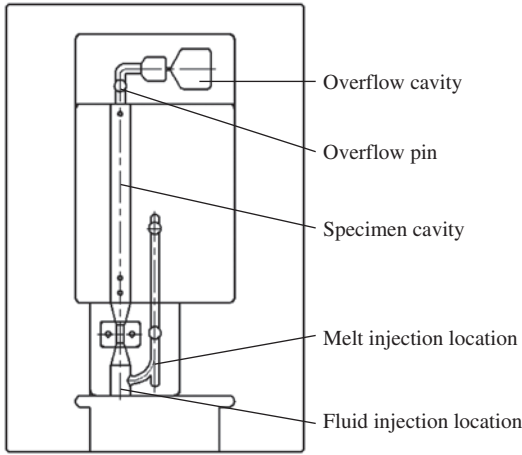
The experiments were carried out on a lab-developed FACIM experimental platform, which comprised an

Table 1: Properties of the high-density polyethylene used in the experiments.

Property	Measure	Value
Tensile yield stress	Q/SY DS 0512	30.4 MPa
Tensile break stress	Q/SY DS 0512	26.3 MPa
Density	Q/SY DS 0510	0.9566 g/cm <sup>3</sup>
Melt flow index	Q/SY DS 0511	7.3 g/10 min
Impact strength	GB/1043.1-2008	5.8 kJ/m <sup>2</sup>

Table 2: Properties of the polypropylene used in the experiments.

Property	Measure	Value
Yield strength	ASTM D-638	52.0 MPa
Bending modulus	ASTM D-790	2850 MPa
Hardness	ASTM D-785	112 R
Heat distortion temp.	ASTM D-648	364 K
Melt flow index	ASTM D-1238	20 g/10 min
Impact strength	ASTM D-256	185 J/m



**Figure 2:** Layout of the mold cavity and various cross-section shapes of the cavities.

injection machine, a water/gas injection unit, a mold with changeable inserts, and a control unit. The molding machine was a 110-ton CIM machine (FB-110C, FCS Group, Taiwan). The lab-developed water injection unit included a plunger water pump with a maximum pressure of 33 MPa, a pressure-regulating valve, a water tank, and a water injection pin. The water injection pin can also be used as the gas injection pin. The switching of the water injection pin was accomplished via a pneumatic control system. The gas injection unit included an air compressor, a nitrogen storage tank, a nitrogen pressure control unit (GPC FX, Hangkong Gas Injection Molding Lt. Co., Hangkong) with a maximum pressure of 35 MPa, and the gas injection pin. The mold was able to accommodate interchangeable inserts to allow for flexibility in specimen geometry. Figure 2 shows the mold with interchangeable inserts. An overflow pin, which was used to disconnect

the part cavity and the overflow cavity, was located at the overflow channel and also controlled by the pneumatic control system. In O-FACIM, the pin was drawn back such that the melt could be pushed into the overflow cavity, while in S-FACIM, the pin was ejected such that the melt could not be pushed into the overflow cavity.

### 2.3 Geometry of the cross-sections of the cavities

Six typical cross-section cavities were selected in this study, and these sections are shown in Figure 3. The lengths of these cavities were 200 mm. All edges of the cavity were filleted with a 2-mm radius. Because the fluid always penetrated along the direction of least resistance, after the delay time, the hottest and lowest viscosity material was likely to be located at the center, which resulted in the least resistance there. Thus, the centers of the inscribed circles of each cross-section were found and marked.

In order to conveniently compare and analyze the cavities, a circle ratio was introduced to characterize these sections. A circle had a maximum circle ratio of 1. Thus, the formula for calculating the circle ratio,  $\alpha$ , was

$$\alpha = \frac{4\pi S}{C^2} \times 100\% \tag{1}$$

where  $S$  denotes the area of the cross-section and  $C$  denotes the circumference of the cross-section.

Geometric data for these sections, such as the area of the cross-section ( $A_{CS}$ ), the maximum distance between the inscribed circle center and the wall ( $Max\_D$ ), the radius of the inscribed circle ( $R_{IC}$ ), and the circle ratio, were calculated and are listed in Table 3. Among these

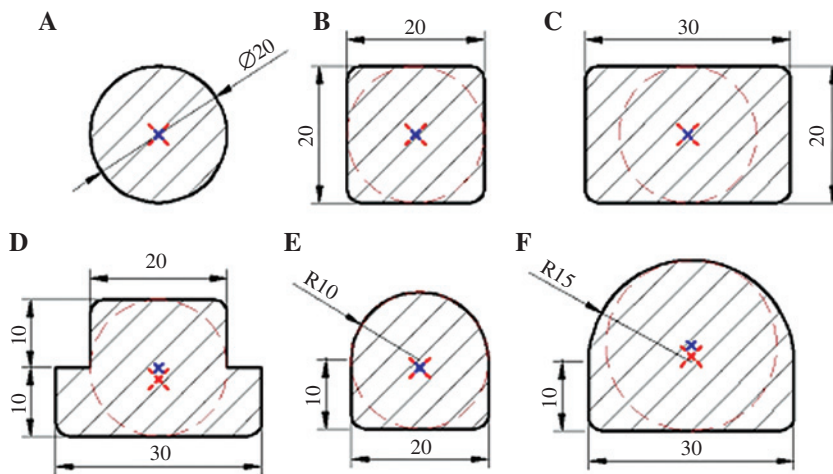


**Figure 3:** Cross-sections of the cavities.

**Table 3:** Geometry of the cross-sections used in the experiments.

Cross-section	$A_{CS}$ (mm <sup>2</sup> )	$Max\_D$ (mm)	$R_{ic}$ (mm)	Circle ratio (%)
(a)	314	10.00	10	100.0
(b)	397	13.31	10	78.5
(c)	597	17.22	10	75.4
(d)	497	17.22	10	62.8
(e)	357	13.31	10	88.0
(f)	653	18.68	12.5	87.0

six cavities, A, B, C, D, and E had the same radius as the inscribed circle, while F had a larger radius. Cavity A had the minimum  $Max\_D$ , while cavity F had the maximum  $Max\_D$ . Cavities B and E had the same  $Max\_D$ , and cavities C and D had the same  $Max\_D$ .

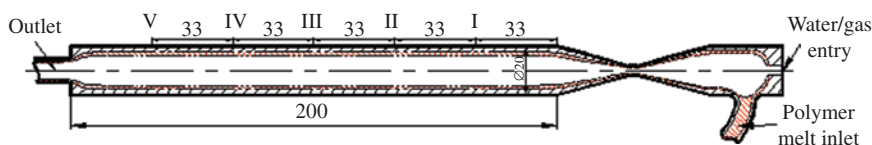
## 2.4 Processing parameters

In order to investigate the influence of fluid on penetration interfaces and make the experimental results comparable, GACIM and WACIM processes were performed using the same processing parameters, which are listed in Table 4. HDPE and PP were used as the outer and inner materials, respectively. The melt injection sequence was reversed to investigate the influence of melt rheology on products with the same processing parameters.

## 2.5 Characterization of molded parts

The circular cross-section specimens obtained were cut in the longitudinal direction, as shown in Figure 4. The total RWT and the RWT of the outer layer were measured at five specified positions (I–V), as shown in Figure 5. The penetration interface fluctuations of the inner melt and the fluid can be seen and evaluated.

All of the cross-section specimens were cut in the transverse direction at the middle position of the specimens. The penetration cross-sections of the inner melt and the fluid can be shown directly. The minimum and maximum values of the total RWT and those of the RWT of the outer layer were measured and averaged from five specimens of each technology at the same processing parameters.

**Figure 5:** Diagram of specimen and measuring positions.**Table 4:** Processing parameters used in the experiments.

Processing parameters	Value
Fluid pressure	4 MPa
Fluid injection delay time	3 s
Outer layer melt temperature	473 K (200°C)
Injection speed of outer layer melt	9.26 cm <sup>3</sup> /s
Outer layer melt inj. volume	85 cm <sup>3</sup>
Inner layer melt temperature	473 K (200°C)
Injection speed of inner melt	9.26 cm <sup>3</sup> /s
Inner layer melt inj. volume	40 cm <sup>3</sup>
Packing time	60 s
Fluid temperature	298 K (25°C)

**Figure 4:** O-FACIM specimens and their cut sections: (A) WACIM and (B) GACIM.

## 3 Results and discussion

### 3.1 Comparison of the RWTs of WACIM and GACIM circular tube specimens

WACIM and GACIM circular pipe specimens with a diameter of 20 mm were cut in the longitudinal direction and are shown in Figure 6. As can be seen, the internal surface

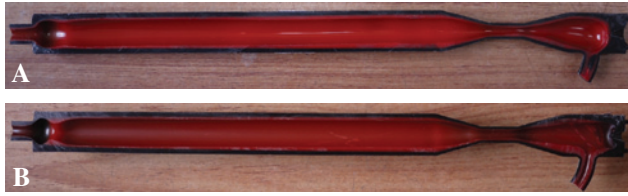


**Figure 6:** Longitudinal sections of FACIM specimens: (A) WACIM and (B) GACIM, outer layer HDPE, and inner layer PP.

**Table 5:** Residual wall thicknesses of WACIM and GACIM specimens.

Position	WACIM			GACIM		
	$R_t$ (mm)	$R_o$ (mm)	$R_i$ (mm)	$R_t$ (mm)	$R_o$ (mm)	$R_i$ (mm)
I	3.42	2.00	1.42	3.34	2.00	1.34
II	3.80	2.12	1.68	3.42	2.10	1.32
III	3.54	2.20	1.34	3.34	2.14	1.20
IV	3.36	2.24	1.12	3.32	2.18	1.14
V	3.26	2.26	1.00	3.28	2.20	1.08

$R_t$  denotes the total RWT,  $R_o$  denotes the RWT of the outer layer, and  $R_i$  denotes the RWT of the inner layer which equals  $R_t$  minus  $R_o$ .

of the WACIM specimen was smoother and brighter than that of the GACIM specimen.

The total RWT and the outer layer thickness at the five specified locations of the WACIM and GACIM specimens were measured, and the values are listed in Table 5.

Based on the data listed in Table 5, the RWT variation in the flow direction of both WACIM and GACIM specimens is shown graphically in Figure 7. At the same processing parameters, the RWT of the outer melt of the WACIM specimens was similar to that of the GACIM specimens and became slightly thicker in the flow direction. This was because the outer melt could not come into contact with the fluid during the filling stage of the O-FACIM process and its RWT was mainly affected by the inner melt penetration. In the GACIM process, the RWT of the inner layer became slightly thinner in the flow direction and the total RWT was rather stable. However, in the WACIM process, the RWT of the inner layer fluctuated and resulted in the fluctuation of the total RWT. This shows that the penetration of water in the inner melt was not stable.

Zhou's research [20] into the interface stability of multiphase stratified flow showed that there was a pair of flow vortices with different sizes and opposite directions in the cross-section of the multiphase stratified flow of polymers with different rheological properties. The strength of the vortex flow and its center position alternated at the interface of the polymers, which led to

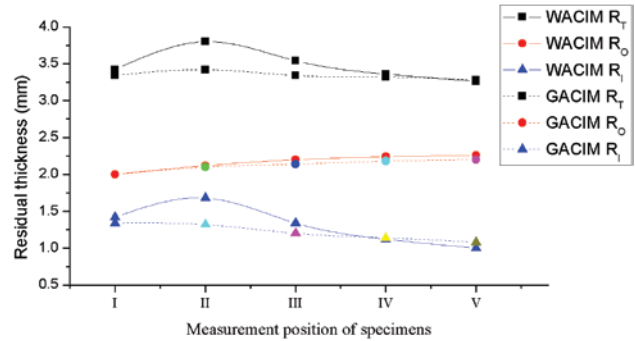


**Figure 7:** Comparison of RWTs between WACIM and GACIM specimens.

interactions at the interface of the two neighboring melts and eventually resulted in unstable three-dimensional flow of multiphase stratified polymer melts. The greater the melt viscosity ratio, the more obvious the interfacial instability became.

Based on this analysis, it can be concluded that, at the same injection rate, the higher the melt viscosity, the greater the flow vortex intensity. Thus, when a higher viscosity melt was used as the inner material, it was prone to dragging the outer melt with the lower viscosity, thus resulting in interface fluctuations. When a lower viscosity polymer was used as the inner melt, it was hard to draw the outer melt with higher viscosity, and hence the interface was relatively stable. This explanation can also be used to explain the phenomenon that in both WACIM and GACIM, no obvious interface instabilities between the outer and inner layers occurred because the inner melt (PP) viscosity was lower than the outer layer (HDPE) melt viscosity (the melt flow indexes of PP and HDPE were 20 and 7.3 g/10 min, respectively), and hence the RWT of the outer layer was uniform.

Furthermore, because the heat capacity of water was approximately 40 times that of nitrogen gas, water had a much stronger cooling capacity than gas. Figure 8 shows the simulation results of the temperature fields near the fluid penetration front. It can be seen that in WACIM, the temperature of the melt near the penetration front was lower due to the fast cooling from the water, while in GACIM, it was almost the same as the temperature of the inside melt due to the poor cooling capacity of the gas. Decreasing the melt temperature increased its viscosity. Thus, the viscosity of the melt near the water was higher than that inside of the inner layer, which resulted in an obvious fluctuation of water penetration. In GACIM, there was no viscosity difference between the melt near the gas and that inside the inner layer, and hence the gas penetration in the inner melt was stable.

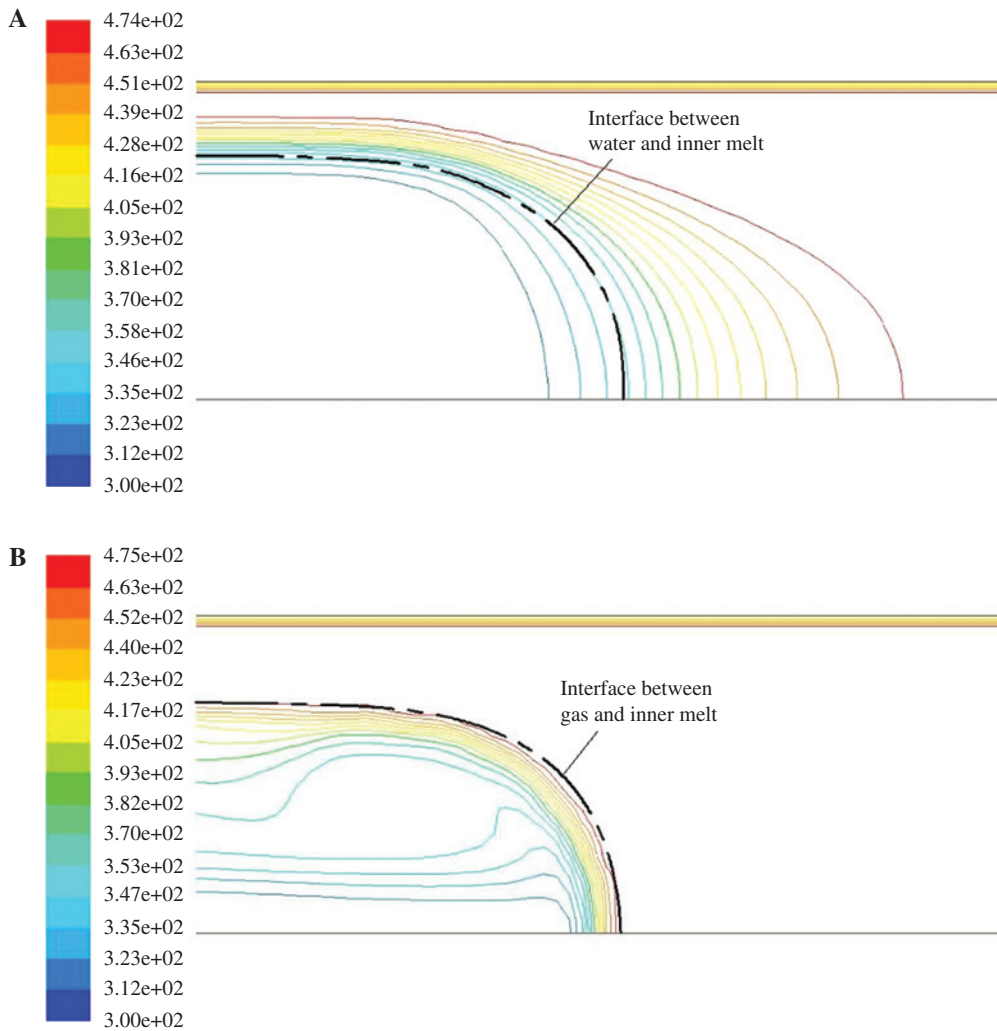


Figure 8: Temperature fields of WACIM and GACIMs: (A) WACIM and (B) GACIM (simulated by ANSYS FLUENT, Cecil Township, PA, USA).

### 3.2 Comparisons of the RWTs of WACIM and GACIM circular tube specimens with a reverse injection sequence

To continue our analysis of WACIM, we reversed the melt injection sequence while keeping the other processing parameters constant. The WACIM and GACIM specimens obtained were cut in the longitudinal direction and are shown in Figure 9.

The total thickness, the outer layer thickness, and the inner layer thickness at the five specified locations of WACIM and GACIM specimens were measured and are shown graphically in Figure 10.

As can be seen, for the WACIM specimens, both the RWTs of the outer layer and the inner layer fluctuated in the flow direction, which resulted in an obvious fluctuation of the total RWT. Meanwhile, for the GACIM

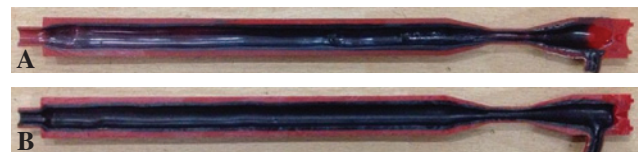


Figure 9: Longitudinal sections of FACIM specimens with a PP outer layer and an HDPE inner layer: (A) WACIM, and (B) GACIM.

specimens, the RWT of the outer layer fluctuated, while the RWT of the inner layer decreased slightly in the flow direction, yielding a fluctuation in the total RWT. Both the RWTs of the outer layers of WACIM and GACIM fluctuated after the injection sequence was reversed. This was because HDPE was used as the inner material, PP was used as the outer material, and the viscosity of HDPE was greater than that of PP. As stated above, the viscosity

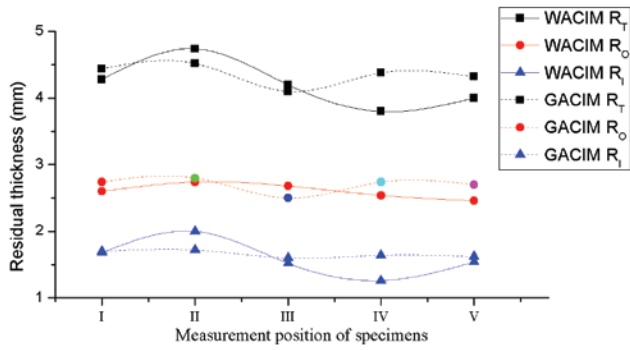


Figure 10: Comparison of RWTs between WACIM and GACIM specimens.

of the inner melt was higher than that of the outer melt, resulting in a fluctuation of the inner-outer interface. Likewise, the RWT of the inner layer in WACIM fluctuated more for the higher viscosity melt near the water as compared to the inside melt.

The experiment with PP as the inner melt and HDPE as the outer melt shows that the RWTs of the outer and inner layers are relatively homogeneous for GACIM, while the RWT of the inner layer fluctuates for WACIM.

It is likely that this result occurs due to the difference in viscosity. Research with other materials with varying viscosities would need to be performed to confirm the result.

### 3.3 Comparison of the penetration sections of WACIM and GACIM specimens

The experimental specimens, produced by O-FACIM under the same processing parameters, were cut into cross-sections at the mid-point of the length of the samples, as shown in Figure 11. In order to conveniently compare the penetration interfaces between GACIM and WACIM, the interfaces were traced and combined together as shown in Figure 12. The penetration areas of water and gas can be calculated by CAD software, and the hollow ratio can be obtained by formula (1). The hollow ratios of the specimens are listed in Table 6. Based on the data listed in Tables 3 and 6, the relationship between the hollow ratio and circle ratio can be obtained, as shown in Figure 13. As can be seen from Figure 12, for the non-circular pipes, both the penetration area of the inner melt and that of the gas in the GACIM specimens were larger than those of the

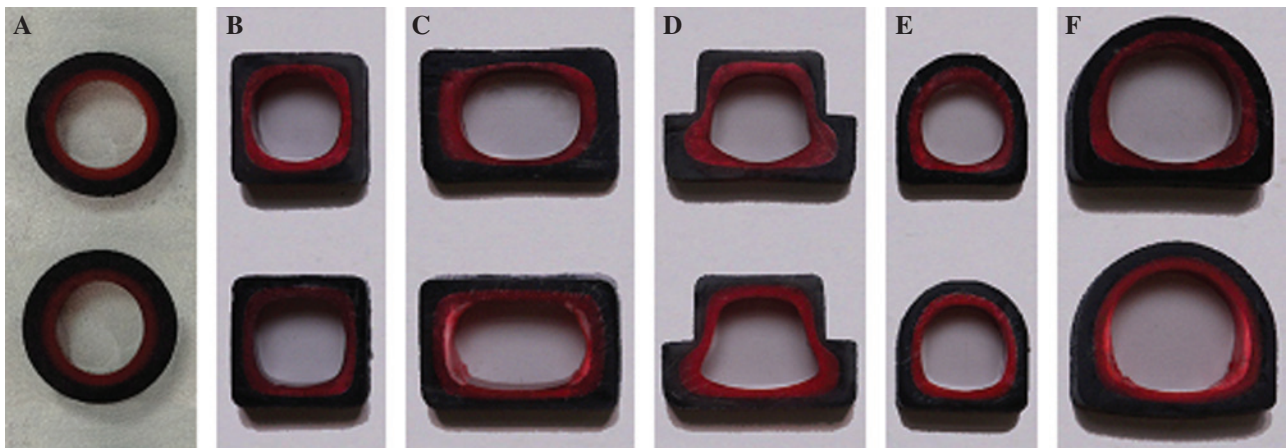


Figure 11: Cross-sections of FACIM specimens: the upper row indicates WACIM, and the lower row GACIM.

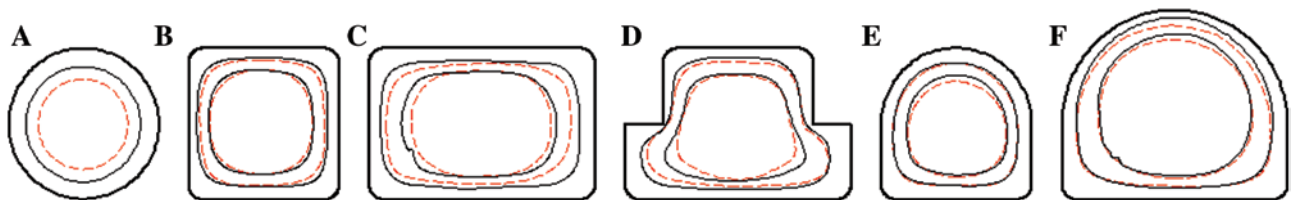
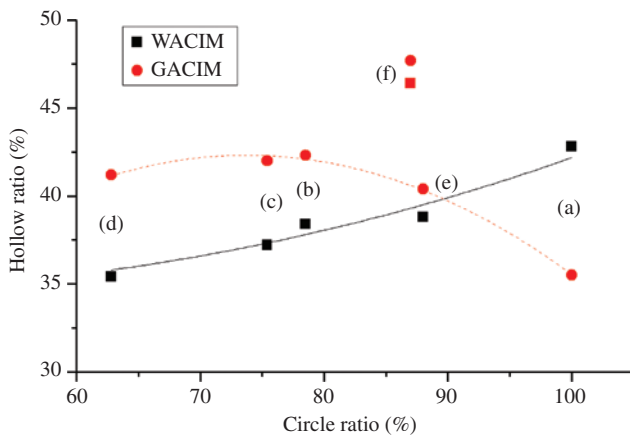


Figure 12: Penetration interfaces of WACIM and GACIM specimens with non-circular sections: the solid line indicates GACIM, the dashed line WACIM, the black line the inner-outer melt interface, and the red line indicates the water-inner melt interface.

**Table 6:** Hollow ratio of O-FACIM specimens with different sections.

Cross-section	Circle ratio (%)	Hollow ratio (%)	
		WACIM	GACIM
(a)	100.0	42.8	35.5
(b)	78.5	38.4	42.3
(c)	75.4	37.2	42
(d)	62.8	35.4	41.2
(e)	88.0	38.8	40.4
(f)	87.0	46.4	47.7



**Figure 13:** The relationship between the hollow ratio and circle ratio.

inner melt and the water in WACIM, especially from the center of the geometry to the distal wall. For the circular pipe, however, there were no obvious differences between the penetration of the melt and the water in WACIM and that of the melt and the gas in GACIM. Figure 14 shows that with the same radius of the inscribed circle, the hollow

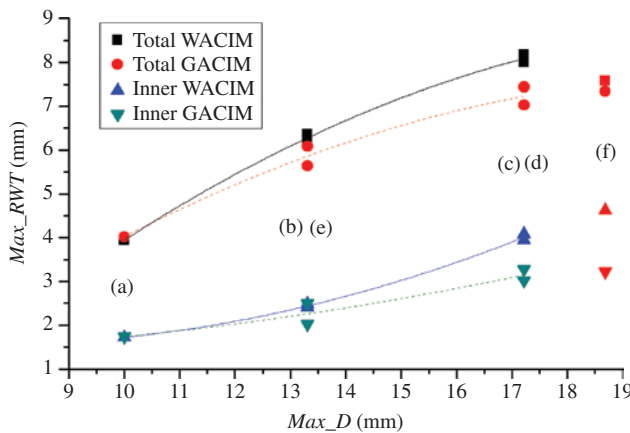


**Figure 14:** The relationship between the maximum RWT and  $Max_D$ .

ratio of WACIM increased with increasing circle ratio and there was no such relationship between the hollow ratio of the GACIM specimen and the circle ratio of the cavity cross-section. This is because in WACIM, the high viscosity layer, which formed at the water penetration front during fast cooling, resulted in a penetration front close to the shape of a ball. Thus, the higher the circle ratio of the cavity cross-section, the higher the hollow ratio of the WACIM specimen. Meanwhile, in GACIM, this phenomenon did not exist due to the poor cooling capacity of the gas. GACIM has a better capability of adapting to the mold cavity and its penetration cross-section is closer to that of the cavity. Cavities E and F had similar circle ratios, while the radius of the inscribed circle of cavity F was 15 mm and that of E was 10 mm, which resulted in the hollow ratio of F being higher than that of E. This was because by increasing the radius of the inscribed circle of the cavity, the relative RWT of the melt decreased and more melt in the core could be pushed out and the hollow ratio increased.

The maximum and minimum total RWT, and the RWT of the inner layer for WACIM and GACIM, were measured and are listed in Table 7. Based on the data listed in Tables 3 and 7, the relationships between the total RWT, the RWT of the inner layer, and the  $Max_D$  can be obtained, as shown in Figures 14 and 15, respectively.

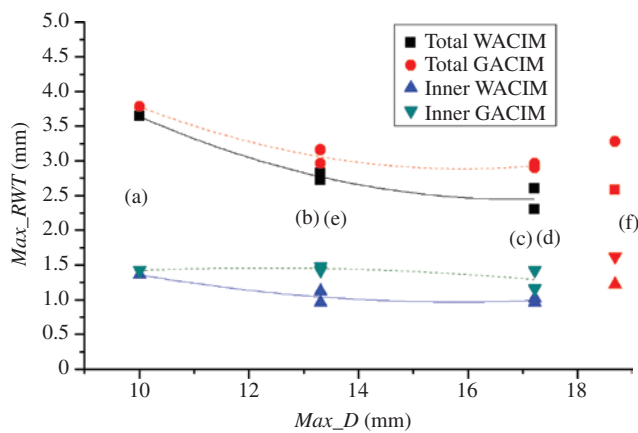
As can be seen for all of these cavities, the maximum total RWT, as well as the RWT of the inner melt of the WACIM specimens, was greater than those of the GACIM samples. Meanwhile, the minimum total RWT and the RWT of the inner melt of WACIM specimens were less than those of the GACIM samples. These results indicated that the uniformity of the total RWT and the RWT of the inner melt of the WACIM specimens were poorer than those of the GACIM samples.

Cavities A, B, C, D, and E had the same radius of the inscribed circle. The maximum and minimum values of the total RWT, and those of the RWT of the inner melt in O-FACIM, for cavities B and E (which had the same  $Max_D$ ), and cavities C and D (which had the same  $Max_D$ ), were very close. Increasing the  $Max_D$  resulted in an obvious increase in the maximum values of the total RWT, and an increase in the RWT of the inner melt of O-FACIM. The minimum values of the total RWT decreased slightly, and those of the RWT of the inner melt remained almost constant. Thus, with the same radius of the inscribed circle,  $Max_D$  had a great effect on the maximum values of the total RWT as well as the RWT of the inner melts in O-FACIM. This was because the minimum RWT always occurred at the nearest wall to the center of the geometry, and the maximum RWT always occurred at the furthest wall to the center of the cross-section.

**Table 7:** RWT of O-FACIM specimens with different sections.

Cross-section	WACIM				GACIM			
	$Max\_R_T$	$Max\_R_I$	$Max\_R_T$	$Min\_R_I$	$Max\_R_T$	$Max\_R_I$	$Min\_R_T$	$Min\_R_I$
(a)	3.94	1.72	3.64	1.36	4.02	1.74	3.78	1.42
(b)	6.20	2.40	2.82	1.12	5.64	2.50	3.16	1.48
(c)	8.00	3.94	2.60	1.02	7.44	3.28	2.96	1.16
(d)	8.18	4.08	2.30	0.96	7.02	3.02	2.90	1.42
(e)	6.38	2.48	2.72	0.96	6.08	2.02	2.96	1.42
(f)	7.58	4.62	2.58	1.22	7.34	3.22	3.28	1.62

$Max\_R_T$  and  $Min\_R_T$  denote the maximum and minimum total RWT, respectively.  $Max\_R_I$  and  $Min\_R_I$  denote the maximum and minimum RWT of the inner layer, respectively.

**Figure 15:** The relationship between the minimum RWT and  $Max\_D$ .

## 4 Conclusions

In this study, an experimental study of the RWT of O-FACIM was carried out based on a lab-developed FACIM system. HDPE and PP were used as the outer layer and inner layer plastics, respectively, in the experiments, and the injection sequence was reversible. Six cross-section cavities were investigated in the experiments. The penetration behaviors of the water and the gas in different sequences and cavities were compared and analyzed. The following conclusions can be drawn from this work. (1) In O-FACIM, if the inner melt viscosity was lower than the outer melt viscosity, the RWT of the outer layer was relatively homogeneous, while the RWT of the inner layer fluctuated due to the fast cooling of the water. The RWT of GACIM was stable. (2) If the inner melt viscosity was higher than the outer melt viscosity, in WACIM, both the RWTs of the outer layer TO and the inner layer TI fluctuated, which resulted in an obvious fluctuation of the

total RWT. Meanwhile, in GACIM, under the same conditions, the RWT of the outer layer TO fluctuated, the RWT of the inner layer TI decreased slightly in the flow direction, and the total RWT fluctuated as well. (3) In general, the higher the circle ratio of the cavity cross-section, the higher the hollow ratio of the WACIM specimen. Compared with WACIM, GACIM had a better ability to adapt to the mold cavity. In addition, its penetration cross-sections were closer to that of the cavity. (4) With the same radius of the inscribed circle,  $Max\_D$  had a great effect on the maximum values of the total RWT as well as the RWT of the inner melts in O-FACIM.

**Acknowledgments:** This study was supported by the National Natural Science Foundation of China (NSFC, No. 51103037) for which the authors are very grateful. This project was also supported by the China Scholarship Council (CSC, 2013), the Science and Technology Association of Jiangxi Province (2014), and the Wisconsin Institute for Discovery (WID) at the University of Wisconsin-Madison.

## References

- [1] Lang S, Parkinson MJ. *Plast. Rubber Compos.* 2005, 34, 232–235.
- [2] Lin K-Y, Liu S-J. *Polym. Eng. Sci.* 2009, 49, 2257–2263.
- [3] Lin K-Y, Chang F-A, Liu S-J. *Int. Commun. Heat Mass Transfer* 2009, 36, 491–497.
- [4] Lin K-Y, Liu S-J. *Macromol. Mater. Eng.* 2010, 295, 342–350.
- [5] Liu SJ, Wu YC. *Polym. Test.* 2007, 26, 232–242.
- [6] Chen YL, Zhou H, Zhang ZM, Kong HZ. *China Plast.* 2012, 26, 72–75.
- [7] Zhang K, Kuang TQ, Liu HS, Zeng XS. *Polym. Mater. Sci. Eng.* 2013, 29, 178–182.
- [8] Seldén R. *Polym. Eng. Sci.* 2000, 40, 1165–1176.
- [9] Kim NH, Isayev AI. *Polym. Eng. Sci.* 2015, 55, 88–106.

- [10] Sun M, Zhou GF, Zhang XX, Pang MJ. *China Plast.* 2003, 17, 87–91.
- [11] Zhou GF, Zhong XG, Zhou YF, Guo JL, Yan L. *China Plast.* 2006, 20, 59–61.
- [12] Zhou WY, Zhou GF. *Light Industry Machinery* 2008, 26, 20–22.
- [13] Yan L. Master thesis, Nan Chang University, Nan Chang Jiang Xi, China, 2007.
- [14] Zhou GF, Chao FC, Zhang Y. *Eng. Plast. Appl.* 2013, 41, 47–49.
- [15] Kuang TQ, Liu HS, Zhou GF, Li GJ. *China Plast.* 2006, 20, 82–85.
- [16] Kuang TQ, Liu HS, Zhou GF. *J. Plast. Eng.* 2007, 14, 134–137.
- [17] Kuang TQ, Deng Y. *China Plast.* 2013, 27, 106–110.
- [18] Zhang K, Kuang TQ, Liu HS, Zeng XS. *Polym. Mater. Sci. Eng.* 2013, 29, 174–177.
- [19] Zhou GF, Sun J, Zhong XG. *Appl. Eng. Plast.* 2007, 35, 27–30.
- [20] Zhou GF. *CIESC J.* 2004, 55, 1174–1178.